scientific reports

Check for updates

OPEN

Phyllanthi Fructus ameliorates hyperuricemia and kidney injure via inhibiting uric acid synthesis, modulating urate transporters, and alleviating inflammation

Shaoyu Liang[1], Dandan Xu[2], Junhong Wu[1], Qianqian Jiang[1]✉ & Yongchang Zeng[3]✉

***Phyllanthi Fructus*, known as Yuganzi (YGZ), is a unique medicine and food homologous fruit with both medicinal and nutritional properties. Its historical use in treating hyperuricemia (HUA) and gout is well-documented. However, the precise therapeutic effects and potential molecular mechanisms remain unclear. In this study, an experimental rat modelling by a high-fat/high-sugar diet and potassium oxonate/adenine oral administration was used to evaluate the pharmacodynamic effects of YGZ. Network pharmacology, molecular docking and molecular dynamics simulation were utilized to elucidate the potential mechanisms. Supplementation with YGZ effectively ameliorated HUA by inhibiting xanthine oxidase activity, and enhancing uric acid excretion through up-regulating of OAT1 and ABCG2, while down-regulating of URAT1. Furthermore, YGZ supplementation enhanced superoxide dismutase activity, reduced malondialdehyde content, and inhibited the secretion of IL1B, IL6, TNFα, ICAM1, VCAM1, TGFβ1, and NF-κB protein expression. Network pharmacology analysis indicated that YGZ influences 138 targets, modulating the disease network via lipid and atherosclerosis, insulin resistance, HIF-1, TNF, IL-17, TLRS, and NF-κB signaling pathways. Molecular docking analysis suggested that organic acids (e.g. ellagic acid, gallic acid) and flavonoids (e.g. quercetin, delphinidin, luteolin, epigallocatechin gallate) exhibited superior binding abilities to key targets (e.g. XDH, ABCG2, URAT1, OAT1, IRS1, PTGS2, TLR4). Noteworthy, molecular dynamics simulations confirmed that epigallocatechin gallate binds to URAT1 with the greatest stability. These results provide substantial evidence for the therapeutic efficacy of YGZ and establish a theoretical foundation for the development of natural products in treating hyperuricemia.**

Keywords *Phyllanthi Fructus*, Hyperuricemia, Urate transporter, Inflammation, Network pharmacology, Molecular docking

Hyperuricemia (HUA) is a metabolic syndrome resulting from a disorder of purine metabolism or decreased excretion of uric acid (UA), which leads to elevated serum level of UA. Globally, the prevalence of HUA has increased substantially over the past decade, with younger onsets[1–3]. Historically, asymptomatic hyperuricemia was regarded as a benign laboratory abnormality with no significant clinical implications[4]. However, mounting evidence indicates that HUA plays an independent role in the development and severity of gout, renal dysfunction, metabolic syndrome, cardiovascular disease[5]. Once diagnosed with HUA, non-pharmacological treatments including maintaining a balanced diet, controlling purine content in dietary intake, restricting daily caloric consumption, consuming fresh vegetables and fruits, engaging in regular physical exercise, and limiting smoking, are preferentially recommended to prevent further progression or deterioration. Nevertheless, when health guidance and lifestyle interventions are ineffective in controlling serum UA level, pharmacological treatments should be adopted to combat HUA. Currently, the UA-lowering therapies are classified into three main categories: xanthine oxidase (XO) inhibitors, uricosuric agents, and recombinant uricase. Although these drugs have been demonstrated to be highly efficacious in reducing serum UA, their potential adverse

[1]The First Affiliated Hospital of Shenzhen University, Shenzhen 518020, China. [2]Guizhou University of Traditional Chinese Medicine, Guiyang 550025, China. [3]The Affiliated TCM Hospital of Guangzhou Medical University, Guangzhou 510000, China. ✉email: jq105@163.com; zyc1199@126.com

reactions are a cause for concern[6–8]. For allopurinol, as the first-line therapy for HUA and gout, the potentially fatal allopurinol hypersensitivity syndrome (AHS) represents a significant and important issue in the initial few months following treatment. As a potent uricosuric agent, benzbromarone is not widely accepted due to its potential hepatotoxicity. Consequently, the development of safe, nontoxic functional foods or dietary supplements for alternative therapy seems to be a matter of particular urgency and importance.

Phyllanthus emblica L., a traditional medicine and food homology (MFH) plant, is widespread throughout subtropical and tropical regions of India and China. All parts of *Phyllanthus emblica* L., including the leaves and bark, have been demonstrated to possess medicinal properties, especially the fruits. *Phyllanthi Fructus*, also known as Yuganzi (YGZ) in Chinese, is the ripe fruit of *Phyllanthus emblica* L., with a distinctive sour-astringent flavor profile and an accompanying sweet aftertaste. Due to the presence of various biologically secondary metabolites (including tannins, phenolic acid, lipids, flavonoids, etc.)[9], YGZ is regarded as possessing considerable pharmacological properties, in addition to its substantial nutritional content. It has been utilized in the development of food, beverages, dietary supplements and cosmetics. In traditional and ethnic medicine, YGZ is believed to possess the capacity to clear heat and cool the blood, strengthen the stomach and promote digestion, stimulate salivation, and relieve coughs[10]. In contemporary pharmacological studies, it has been demonstrated to have an important impact on the regulation of blood glucose and lipid metabolism, providing anti-inflammatory, anti-cancer, anti-oxidant, and anti-atherogenic functions[11–15]. Moreover, YGZ has been used for treating gout for centuries in Tibetan medicine. Recent pharmacological studies have demonstrated that YGZ possesses excellent anti-HUA and gout properties, particularly in the inhibition of XO activity and anti-inflammatory effects[16,17]. Nevertheless, there is a paucity of studies that have investigated the potential impact of YGZ on UA transporters modulation, despite the fact that UA transporters play a more critical role in maintaining the balance of the UA pool. As a multi-ingredient centered nutritional supplementation, the comprehensive role of YGZ remains a mystery.

Considering the intricate characteristics of natural medicinal plants, we employed pharmacological experiment, network pharmacology, molecular docking, and molecular dynamics simulations to predict the therapeutic effects and underlying mechanisms of YGZ in treating HUA and gout. A HUA rat model, induced by a high-fat/high-sugar diet and oral administration of potassium oxonate/adenine, was employed to analyse the therapeutic effect of YGZ on a range of clinical biochemical indexes, cytokine levels, XO activity, and histopathological changes in the liver and kidney, with a particular focus on UA transporter expression. Subsequently, network pharmacology was performed to investigate the underlying molecular mechanisms. Finally, the key proteins highly associated with HUA and gout, as well as the core active components, were validated through molecular docking and molecular dynamics simulations. The systematic research described above not only illuminated the molecular mechanisms of YGZ in treating HUA and gout, but also provided theoretical foundations for the development of natural products in treating HUA. The workflow is depicted in Supplementary Fig. 1.

Materials and methods

Chemicals and reagents

Phyllanthi Fructus was purchased from Shao Huatang Chinese Medicine Co., LTD (Anhui, China) and identified by Professor Chuanming Liu of College of Traditional Chinese Medicine, Southern Medical University. Standards of gallic acid, catechin, corilagin and ellagic acid were provided by Shanghai Yuanye Biotechnology Co., Ltd (Shanghai, China), with a purity greater than 95%. Potassium oxonate (PO), adenine (ADE) and benzbromarone (BEN) were obtained from Sigma-Aldrich (St. Louis, MO, USA). MDA, SOD, IL1B, IL6, TNFα, TGFβ1,VCAM1, and ICAM1 assay kits were provided by Nanjing Senbeijia Biological Technology Co., Ltd. (Nanjing, China). XO assay kits were provided by Jiancheng Biotechnology Institute (Nanjing, China). Urate stain kits were purchased from Beijing Solarbio Science & Technology Co., Ltd. (Beijing, China). The primary antibodies, including anti-URAT1, anti-OAT1, anti-ABCG2 and anti-NF-κB were provided by Bioworld Technology (Nanjing, China).

Preparation of *Phyllanthi Fructus* (YGZ) extract

Briefly, *Phyllanthi Fructus* was dried, pulverized, and soaked in distilled water at a ratio of 1:10 (weight/volume) for 30 min. Thereafter, the mixture decocted twice for 60 min each. The resulting filtrates were collected and concentrated under vacuum to yield a YGZ solution with a concentration of 1 g/mL.

High performance liquid chromatography analysis of YGZ extract

HPLC analysis was performed using the SHIMADZU Prominence-i LC-2030 series HPLC system (SHIMADZU, Japan), equipped with a Supersil ODS2 column (250 mm × 4.6 mm, 5 μm). The mobile phase was composed of acetonitrile (A) and 0.2% (v/v) formic acid aqueous (B). A gradient elution method with a flow rate of 1.0 mL/min, was employed according to the following procedure: 0 ~ 10 min, 2 ~ 5% A; 10 ~ 22 min, 5 ~ 10% A; 22 ~ 42 min, 10 ~ 15% A; 42 ~ 52 min, 15 ~ 22% A; 52 ~ 60 min, 22 ~ 50% A; 60 ~ 65 min, 50 ~ 2% A. The column was maintained at a tempeerature of 25 ℃, an injection volume was set to 10 μL, while the detection wavelength remained at 215 nm.

Pharmacodynamic evaluation of YGZ for the treatment of HUA

Animals and prescription administration

Six-to-eight-week-old male Sprague–Dawley rats, with a weight range of 180–220 g, were purchased from Zhuhai Baishitong Biotechnology Co. LTD (No.SCXK(Yue) 2020–0051). Prior to the commencement of any experimental procedure, all rats were maintained in specific pathogen-free conditions at a temperature of 22–28 °C and a humidity of 55–65%, in 12-h cycles with a 12-h light/dark cycle.

After one week of acclimatization, 24 rats were randomly assigned to 4 groups (n = 6 per group): control group (CON), HUA model group (MOD), YGZ group (YGZ, 0.81 g/kg/d) and benzbromarone group (BEN, 9.0 mg/kg/d) (as shown in Fig. 1). The procedure used to create the HUA rats was conducted in accordance with the methodologies delineated in the pertinent literature[18–21], with minor modifications. A high-fat/high-sugar diet combined with potassium oxonate/adenine oral administration was employed to prepare HUA rats. With the exception of the CON group, all animals in the MOD, YGZ, and BEN groups were subjected to a high-fat/high-sugar diet and orally administered a suspension of potassium oxonate (PO, at a dosage of 1.0 g/kg) and adenine (ADE, at a dosage of 50 mg/kg) for four weeks. The rats in the CON group were maintained on a standard diet and received an equivalent volume of vehicle via gavage. Two hours post-modeling with PO/ADE, animals in each experimental group were orally administered the respective drugs, while rats in the CON and MOD groups were given equal volumes of vehicle instead. The dosages of YGZ and BEN were calculated based on the clinical dosages of 9 g/d and 100 mg/d, respectively.

Oral glucose tolerance test (OGTT)

An oral glucose tolerance test was performed to assess the improvement in glucose metabolism following a four-week supplementation with YGZ. Basal blood glucose levels were measured after a 12-h fast. A glucose solution was administered orally at a dosage of 2 g/kg. Following administration, the blood glucose levels were quantified via the caudal veins at 30, 60 and 120 min. The glucose's area under the curve (AUC) was calculated via the trapezoidal rule.

Sample collection

On the 28th day, all experimental rats were anesthetized via inhalation with an excessive dosage of the inhaled anesthetic isoflurane. Blood samples were obtained from the abdominal aorta, and subsequently processed through centrifugation at 3500 rpm for 10 min. The resulting serum was then separated and cryopreserved at − 80℃ for further analysis. The spleen, liver and kidney were collected, weighed, and the viscera indexes were calculated. One section of the kidney and liver was fixed in 4% paraformaldehyde for sbsequent hematoxylin and eosin (H&E) staining and immunohistochemical analysis, while one section of the kidney underwent fixation in anhydrous ethanol for silver hexamine staining. The remainder kidney and liver samples were stored in liquid nitrogen for subsequent analysis.

Biochemical indexes, oxidative stress, cytokine level and xanthine oxidase activity analysis

The serum levels of UA, fasting blood glucose (FBG), triglycerides (TG), total cholesterol (TCHO), high-density lipoprotein cholesterol (HDL-C), low-density lipoprotein cholesterol (LDL-C), blood urea nitrogen (BUN), and creatinine (Cr) were quantified using a biochemical analyzer. The levels of maleicdialdehyde (MDA), superoxide dimutase (SOD) in serum, the concentrations of IL-6, IL-1β, TNF-α, TGF-β1, VCAM-1 and ICAM-1 in kidney, as well as the XO activity in liver were measured using ELISA kits.

Histopathology of kidney and liver tissues

The kidney and liver tissues were preserved by fixation in 4% paraformaldehyde, followed by embedding, sectioning, and finally staining with hematoxylin and eosin. The image of the section was captured using the SQS-40P slide scanner system (Teksqray, Shenzhen, China).

Gomori's methenamine silver stain for urate crystals in kidney tissues

The kidney tissues were preserved in absolute alcohol, embedded in paraffin wax, and sliced into sections measuring 4–5 μm. Then the sections were subjected to de-paraffination, a process involving the removal of the paraffin used during embedding in xylene and subsequent rinsing in absolute alcohol. Subsequently, the sections

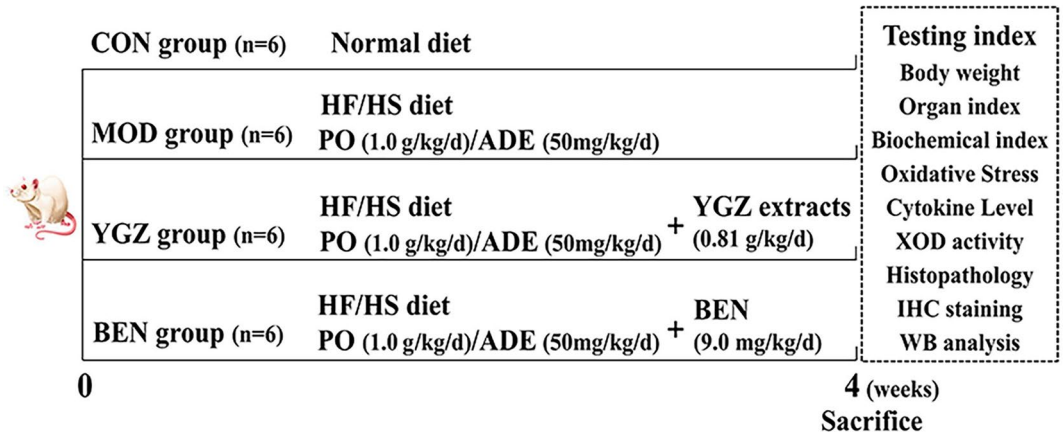

Fig. 1. The outline of the experimental procedure. HF/HS diet: high-fat/high-sugar diet; PO/ADE: potassium oxonate and adenine oral administration; YGZ: Yuganzi extracts; BEN: benzbromarone.

were subjected to a preheated working methenamine silver solution, followed by a gold chloride toning agent and a counterstain with eosin solution. The urates will be stained a distinct brownish-black color.

Immunohistochemical staining

Immunohistochemistry (IHC) was used to analyze the expression of OAT1 and NF-κB p65 in the kidney tissue. Paraffin sections were incubated with primary antibodies OAT1 and NF-κB p65 overnight at 4℃. Subsequently, the sections were incubated with secondary antibodies at room temperature. Thereafter, the positive expression was visualized by a DAB kit. Finally, all the sections were counterstained with haematoxylin. All slices were scanned and images were recorded with ImageViewer (DPVIEW V2.0.4.0531) software. The positive area was quantitatively analyzed using ImageJ software.

Western blot analysis

The total protein extraction from the kidney was conducted via the RIPA lysis buffer extraction method. The extracts underwent centrifugation at 12,000 g for 10 min. Thereafter, the protein content of the resulting supernatants was evaluated via a BCA assay kit. Samples of equal protein quantity were subjected to 10% SDS-PAGE separation, followed by electrophoretic transferring to a PVDF membrane. Nonspecific binding sites on the membranes were blocked by NcmBlot blocking buffer. The membranes were incubated with primary antibodies URAT1 and ABCG2, at 4 ℃ overnight. Following three washes with TBST, the membranes were incubated with HRP-conjugated secondary antibodies at room temperature for 1 h. Finally, the protein bands were visualized using the ECL method and analyzed with Image J software.

Statistical analysis

All data were presented as mean ± standard deviation (SD). The significance of the differences between the means were evaluated by one-way analysis of variance (ANOVA) using SPSS (version 20.0, IBM, United States). The criterion for statistical significance was set at a probability value of $p < 0.05$.

Ethics approval and consent to participate

The animal procedure received ethical approval from the Animal Ethics Committees of Rui Ye Model Animal (Guangzhou) Biotechnology Co., LTD (NO.20211210). The study was conducted in accordance with the ARRIVE guidelines and all methods were performed in accordance with the relevant guidelines and regulations.

Network pharmacology analysis

Collection of active components and therapeutic targets of YGZ

The chemical components of YGZ were obtained from Traditional Chinese Medicine System Pharmacology Database (TCMSP, https://old.tcmsp-e.com/tcmsp.php) and literature sources. Candidate components with oral bioavailability (OB) of at least 20% and drug-likeness (DL) of at least 0.10 were selected for further investigation.

The candidate targets of YGZ were identified using TCMSP, Similarity Ensemble Approach (SEA, https://sea.bkslab.org/), and Swiss Target Prediction (http://www.swisstargetprediction.ch/). Following the removal of duplicates, the related targets, which were restricted to the species "Homo sapiens", were standardized to their official symbols using the UniProt database (https://www.uniprot.org/).

Collection of therapeutic targets for HUA and gout

A systematic search for HUA and gout-related targets was conducted through three public databases, including GeneCards (https://www.genecards.org/), DisGeNET (https://www.disgenet.org/),and Therapeutic Target Database (https://db.idrblab.org/ttd/).

Network construction and central network topological analysis

To comprehensively clarify the molecular mechanism of YGZ in treating HUA and gout, the candidate targets of YGZ, and the targets associated with HUA and gout, were submitted to the online jvenn mapping platform (https://jvenn.toulouse.inrae.fr/app/index.html) to generate a venn diagram with confidence. The overlapping genes were identified as potential targets of YGZ for the treatment of HUA and gout. These genes were subsequently imported into the STRING database (https://cn.string-db.org/) using a high confidence score of ≥ 0.7. The "component-target" (C-T) network and protein–protein interactions (PPI) network were visualized using the Cytoscape v3.9.1 software. Four topological parameters, namely maximal clique centrality (MCC), degree centrality (DC), betweenness centrality (BC), and closeness centrality (CC) were calculated to evaluate the central characteristics of each node.

GO and KEGG enrichment analysis[22,23]

Gene Ontology (GO)enrichment analysis was conducted using ClueGO (a Cytoscape plug-in), while Kyoto Encyclopedia of Genes and Genomes (KEGG) pathway enrichment analysis was performed using the DAVID database (https://david.ncifcrf.gov/). Statistically significant GO terms and KEGG pathways were identified based on a *p*-value of less than 0.05.

Molecular docking

In this study, a molecular docking was conducted to investigate the interaction between core components and hub genes. The chemical structures of the bioactive components were obtained from the PubChem database (https://pubchem.ncbi.nlm.nih.gov/), and stored as ligand in SDF format. The 3D crystal structures of the hub proteins, which obtained from Protein Data Bank database (http://www.rcsb.org/pdb) or AlphaFold Protein Structure Database (https://www.alphafold.ebi.ac.uk/), underwent preprocessing, optimization, and minimization

processes, finally saved as receptors. Molecular docking analysis was conducted using Schrödinger Maestro software suite (version 11.1, Schrödinger, L.L.C.). The docking score and the formation of hydrogen bonds within the ligand-receptor complex were evaluated comprehensively to ascertain the final, stable conformation.

Molecular dynamics simulation

Molecular dynamics simulations were conducted to identify the optimal conformations for molecular docking between the selected components and targets using the GROMACS 2022 software. The GAFF and Amber99sb-ildn force field were selected for ligands and the receptor, respectively. The proteins were solvated in cubic boxes of 88,090 TIP3P water molecules, situated at a minimal distance of 1.2 nm from the box edges. Five negative (Cl^-) ions were added to the system to achieve neutralization. The steepest descent method was applied to energy minimization, followed by a 100 ps canonical ensemble (NVT) equilibration, a 100 ps constant-pressure and constant-temperature (NPT) equilibration, in that order. The temperature was maintained at 300 K, and the pressure was set at 1 bar throughout the duration of each simulation. Subsequently, a 100-ns molecular dynamics (MD) production run was conducted, and the root mean square deviation (RMSD), root mean square function (RMSF), radius of gyration (Rg), and hydrogen bonding (H-bond) were calculated to assess the stability of the compound-protein complexes. Additionally, MM-PBSA analysis was performed to determine the free energy of binding between the protein and the molecular ligand.

Results

Content analysis of multiple bioactive components in YGZ extract

The bioactive components of YGZ were characterised by HPLC in comparison with standards. As shown in Fig. 2, four components including gallic acid (77.1 mg/g), catechin (6.8 mg/g), corilagin (9.2 mg/g) and ellagic acid (7.6 mg/g) were identified as the dominant components in YGZ.

Effects of YGZ on body weight and organ index in HUA rat

As depicted in Fig. 3A, the body weight of rats in different experimental groups showed a progressive increase over time. However, the MOD group demonstrated a slower rate of weight gain, compared to the CON group,

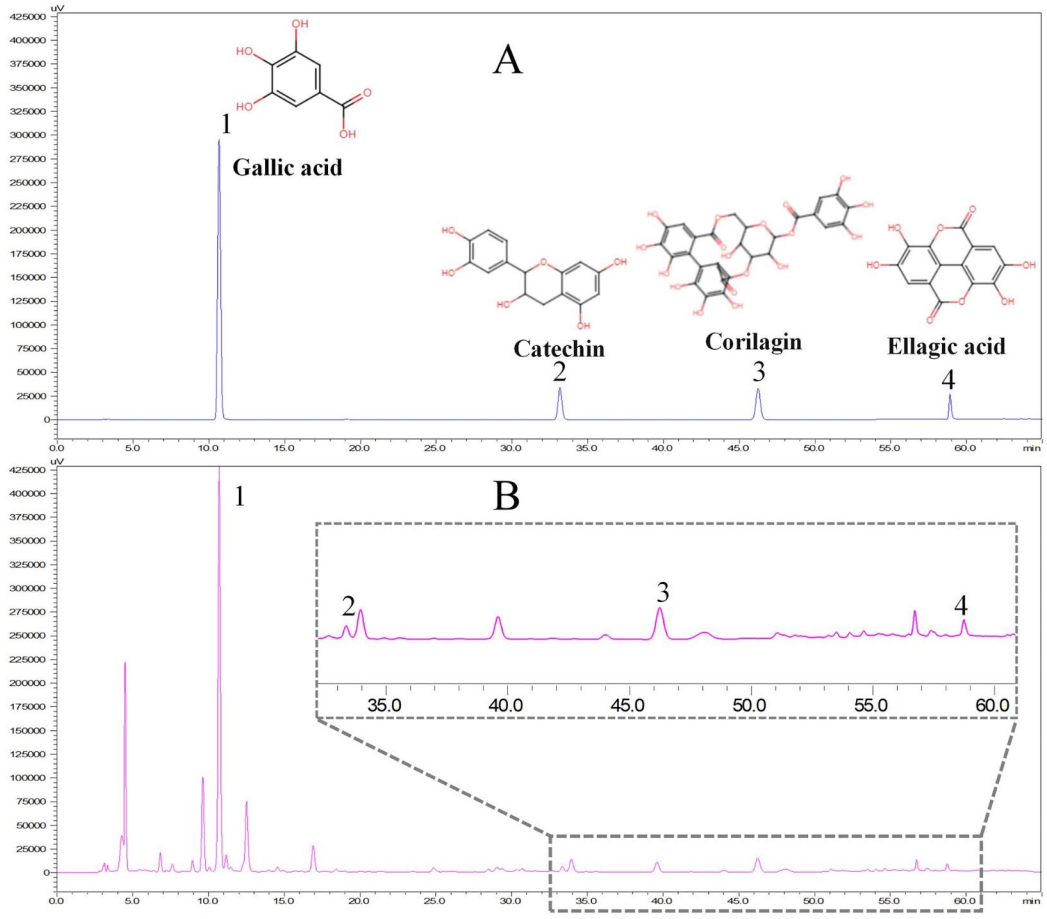

Fig. 2. The HPLC chromatograms of reference substance (**A**) and YGZ extract (**B**) at 215 nm. 1-gallic acid, 2-catechin, 3-corilagin, 4-ellagic acid.

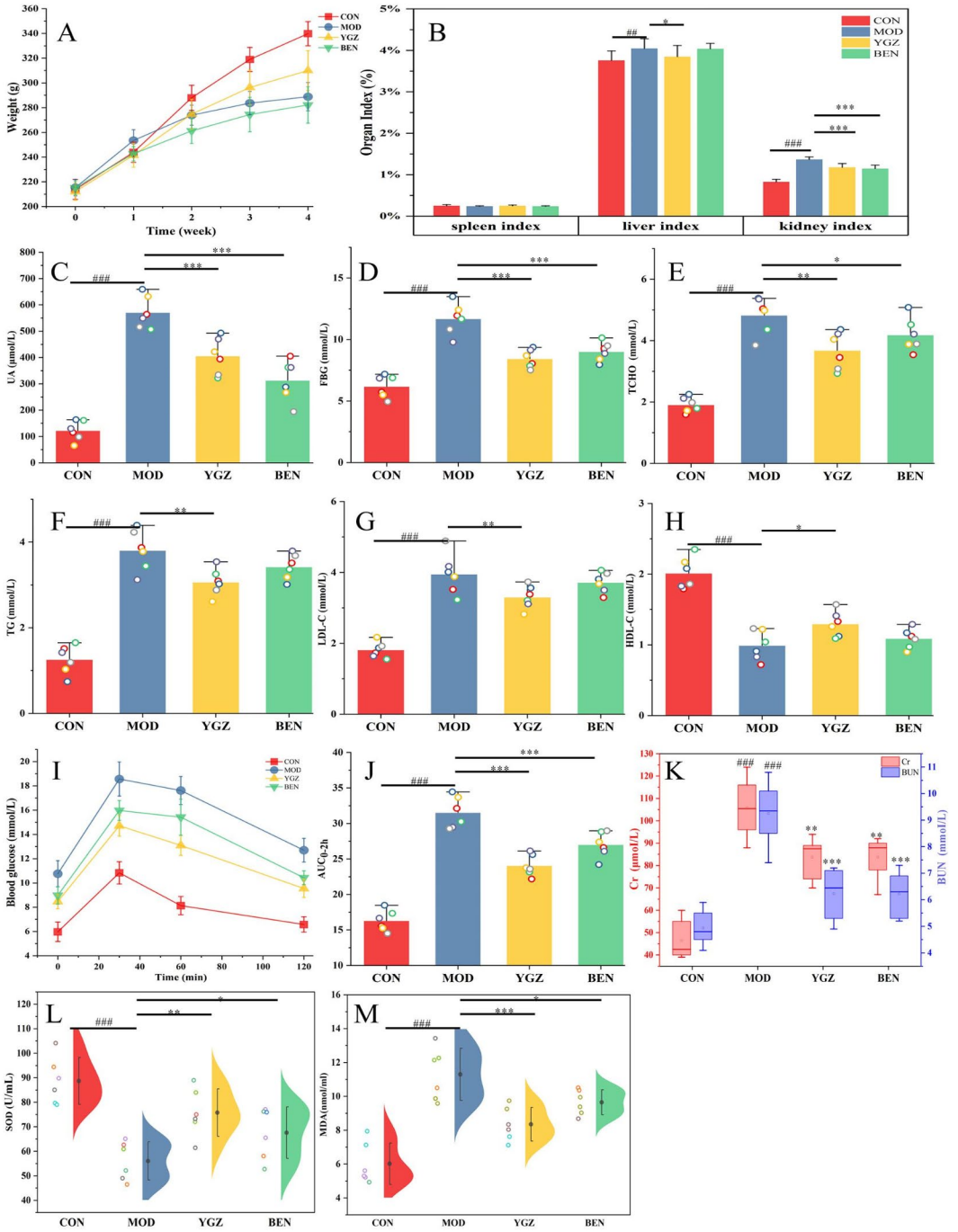

Fig. 3. Effects of YGZ extract on weight (**A**), viscera index (**B**), sUA (**C**), FBG (**D**), TCHO (**E**), TG (**F**), LDL-C (**G**), HDL-C (**H**), glucose curve (**I**), $AUC_{0\text{-}2\,h}$ (**J**), Cr and BUN (**K**), SOD (**L**), MDA (**M**) in HUA rats (Supplementary Tables 1–6). Supplementation with YGZ extracts normalized the reduced weight gain in HUA rats induced by high-fat/high-sugar diet and PO/ADE oral administration, reversed the rise of liver and kidney indexes, reduced the concentrations of UA, FBG, TCHO,TG, LDL-C,Cr, BUN, and MDA, increased the level of HDL-C and the activities of SOD, and enhanced glucose tolerance. Data represented as mean ± SD of 6 rats. $^{\#\#\#}p < 0.001$, $^{\#\#}p < 0.01$, $^{\#}p < 0.05$ vs. CON group. $^{***}p < 0.001$, $^{**}p < 0.01$, $^{*}p < 0.05$ vs. MOD group.

despite being fed a high-fat/high-sugar diet. Supplementation with YGZ partially restored and normalized the reduced weight gain observed in HUA rats.

As illustrated in Fig. 3B, the consumption of a high-fat/high-sugar diet and oral administration of PO/ADE led to a notable elevation in liver and kidney indexes, compared to the CON group ($p < 0.01$). Conversely, supplementation with YGZ resulted in a substantial reduction in liver and kidney indexes (vs. MOD, $p < 0.05$). No significant differences in spleen index was observed among the experimental groups.

Effects of YGZ on serum metabolic indicators, OGTT level and renal function in HUA rat

A prolonged consumption of a high-fat/high-sugar diet may result in metabolic changes. In this study, the purine metabolite (UA), glucose metabolism marker (FBG), and lipid profiles (TG, TCHO, HDL-C, LDL-C) were simultaneously detected to evaluate the effect of YGZ. As showed in Fig. 3C–H, in comparison to the CON group, the serum levels of UA, FBG, TG, TCHO, and LDL-C were markedly elevated in the MOD group, while the level of HDL-C decreased ($p < 0.001$). Supplementation with YGZ led to a notable reduction in the concentrations of UA, FBG, TCHO,TG, and LDL-C (vs. MOD, $p < 0.01$), with a reduction of 28.95%, 27.84%, 23.81%, 19.42%, and 16.46%, respectively. Conversely, YGZ significantly increased the level of HDL-C (vs. MOD, $p < 0.05$). These findings demonstrated that YGZ effectively regulates metabolic processes associated with purine, glucose and lipids in HUA rats.

The alterations in blood glucose levels and the $AUC_{0\text{-}2\ h}$ of blood glucose from 0 to 2 h after oral glucose administration were shown in Fig. 3I–J. In comparison to the CON group, the rats in the MOD group exhibited a higher peak value, a slower decline, and a larger $AUC_{0\text{-}2\ h}$ in their blood glucose levels. Notably, supplementation with YGZ resulted in a lower blood glucose peak and a smaller $AUC_{0\text{-}2\ h}$ (vs. MOD, $p < 0.001$). The results indicated that YGZ can significantly enhance glucose tolerance, in accordance with the findings of previous studies[13].

The accumulation of UA in the kidney can progress to renal damage. In this study, two major indicators of kidney injury, Cr and BUN were examined to evaluate the effects of YGZ on kidney protection. As displayed in Fig. 3K, compared to the CON group, the levels of Cr and BUN in MOD group exhibited a notable elevation, by approximately 2.28 and 1.88 folds, respectively ($p < 0.001$). Supplementation with YGZ extract achieved significant reductions in the levels of Cr and BUN, with a 20.94% reduction in Cr levels (vs. MOD, $p < 0.01$) and a 32.62% reduction in BUN levels (vs. MOD, $p < 0.001$), respectively. YGZ extract exhibits a pronounced protective effect on the kidney.

Effects of YGZ on antioxidative stress ability in HUA rats

UA is a particular molecule exhibiting both antioxidant and pro-oxidant characteristics. A significant elevation in UA concentrations was documented to promote renal oxidative stress. Furthermore, the accumulation of lipids induced by high-fat and high-sugar diets exacerbated the generation of lipid peroxidation and reactive oxygen species. As anticipated, compared to the CON group, the SOD activities were significantly lower in the MOD group, while the MDA levels were prominently higher ($p < 0.001$) (Fig. 3L–M). Administration of YGZ extract conspicuously enhanced the activities of SOD and decreased the level of MDA (vs. MOD, $p < 0.01$). YGZ contributes to the alleviation of lipid peroxidation and oxidative stress caused by HUA.

Effects of YGZ on liver and renal histopathological changes in HUA rats

As shown in Fig. 4A, the hepatocytes in the CON group displayed normal morphology and arrangement, exhibiting a complete and transparent tissue structure with no apparent pathological abnormalities. In contrast, the hepatocytes in the MOD group exhibited notable swelling, vacuolar degeneration, and the presence of dispersed lipid droplets within the cytoplasm, accompanied by a disorganized arrangement of hepatic cords. Supplementation with YGZ extract significantly reduced hepatocyte steatosis and swelling.

As illustrated in Fig. 4B, the renal tubules in the CON group exhibited clear boundaries and neatly arranged epithelial cells. The rats in the MOD group exhibited significant renal pathological changes, including glomerular atrophy and deterioration, vacuolar degeneration in renal tubular epithelial cells, cellular swelling, and severe luminal dilatation. Supplementation with YGZ resulted in a notable improvement in the histological appearance of renal tissue lesions. In particular, the expansion of renal tubular lesions was significantly diminished, accompanied by a remarkable improvement in interstitial atrophy.

As illustrated in Fig. 4C, in the CON group, there were minimal urate crystal formation observed in renal tissues. In contrast, the MOD group exhibited a notable presence of MSU crystals, appearing as brownish-black aggregates within the kidney tissue. Supplementation with YGZ extract resulted in a substantial reduction in MSU crystals.

Effects of YGZ on cytokines in kidney

Previous research has demonstrated that both urate crystals and soluble UA activate the innate immune response by triggering inflammasome pathways, thereby leading to the release of cytokines. As illustrated in Fig. 5A–F, compared to the CON group, a pronounced elevation in the levels of IL-6, IL-1β, TNF-α, ICAM-1, VCAM-1, and TGF-β1 was observed in the MOD group ($p < 0.001$). Supplementation with YGZ extract significantly reduced the secretion of IL-6, IL-1β, TNF-α, ICAM-1, VCAM-1 and TGF-β1 in the kidney, with a reduciton of 22.47%, 28.93%, 28.33%, 20.07%, 21.63% and 21.14%, respectively (vs. MOD, $p < 0.01$).

NF-κB participates in multitude of physiological and pathological processes, including inflammatory response, oxidative stress, immune response, and apoptosis. Long-term exposure to high levels of UA promotes the activation of NF-κB signaling pathways in kidney. As shown in Fig. 5G, compared to the CON group, the MOD group demonstrated a significantly elevated protein expression level of NF-κB p65 ($p < 0.001$). Notably, YGZ administration attenuated the HUA-induced elevation of NF-κB p65 expression (vs. MOD, $p < 0.001$).

Effects of YGZ on UA production and excretion in HUA rats

As shown in Fig. 6A, compared to the CON group, the hepatic XO activity of MOD group showed approximately 1.5-folds higher (13.35 vs 9.03 U/g protein, vs. CON, $p < 0.001$). Supplementation with YGZ led to a reversal of the elevated XO activity, reducing it to 10.49 U/g protein (vs. MOD, $p < 0.001$). YGZ exhibits a significant inhibitory effect on XO activity, thereby reducing UA production.

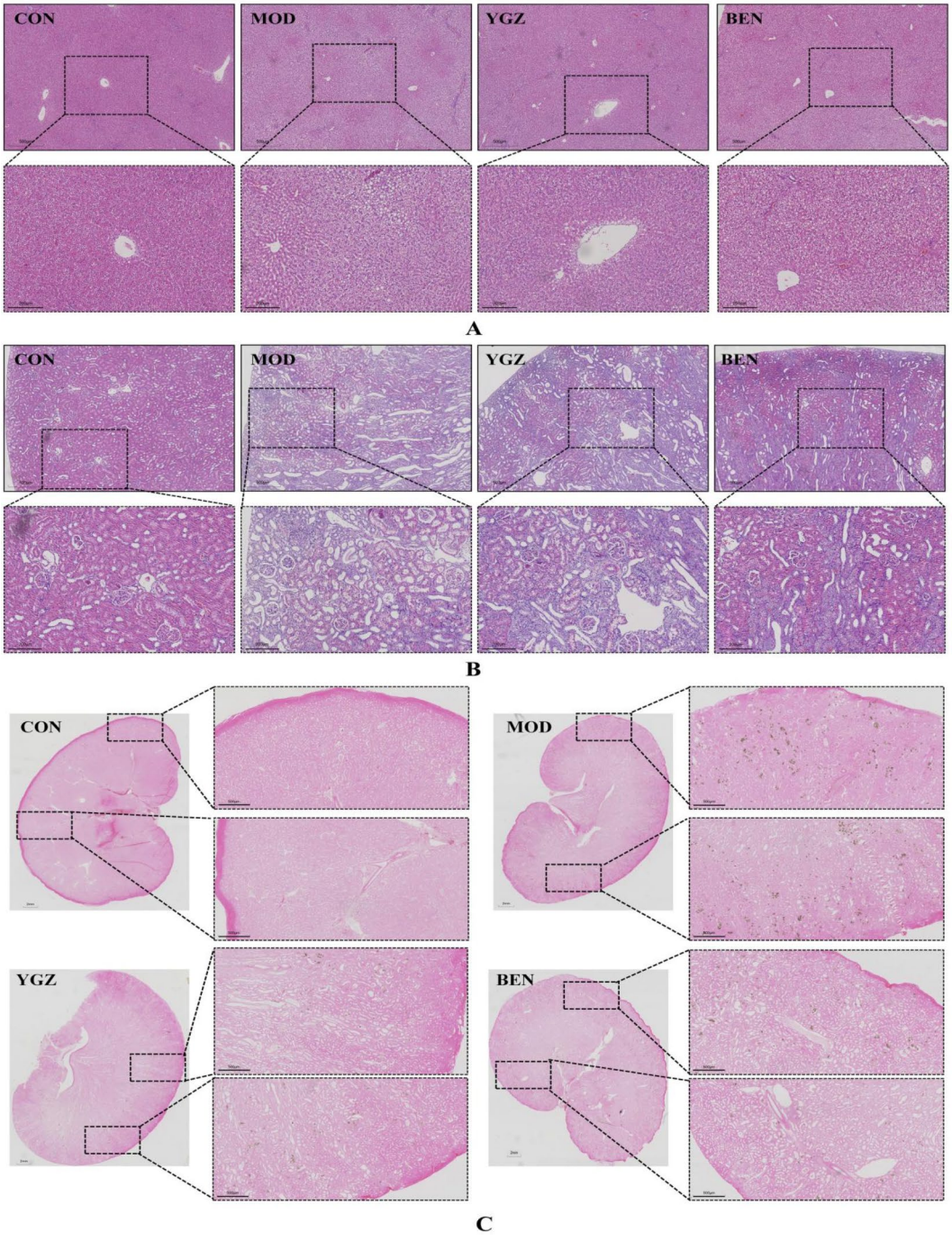

Fig. 4. Histopathological sections of liver and kidney. (**A**) H&E stain sections of liver (100×, scale bar 200 μm), (**B**) H&E stain sections of kidney (100 ×, scale bar 200 μm), (**C**) Gomori's methenamine silver stain sections of kidney (40×, scale bar 500 μm). Supplementation with YGZ extract significantly reduced hepatocyte steatosis and swelling, diminished the expansion of renal tubular lesions and improved the interstitial atrophy, reduced the MSU crystals aggregates within the kidney tissue.

URAT1 play a pivotal role in UA reabsorption, while OAT1 and ABCG2 are responsible for UA excretion. As shown in Fig. 6B–E, in comparison to the CON group, the protein expressions of URAT1 were notably elevated in MOD group ($p < 0.001$), while those of ABCG2 and OAT1 were significantly decreased ($p < 0.001$). Supplementation with YGZ extract was found to significantly reverse the up-regulation of URAT1, as well as the down-regulation of ABCG2 and OAT1 (vs. MOD, $p < 0.05$). YGZ exerts an inhibitory effect on UA reabsorption, simultaneously promoting its secretion, which ultimately leads to enhance UA excretion.

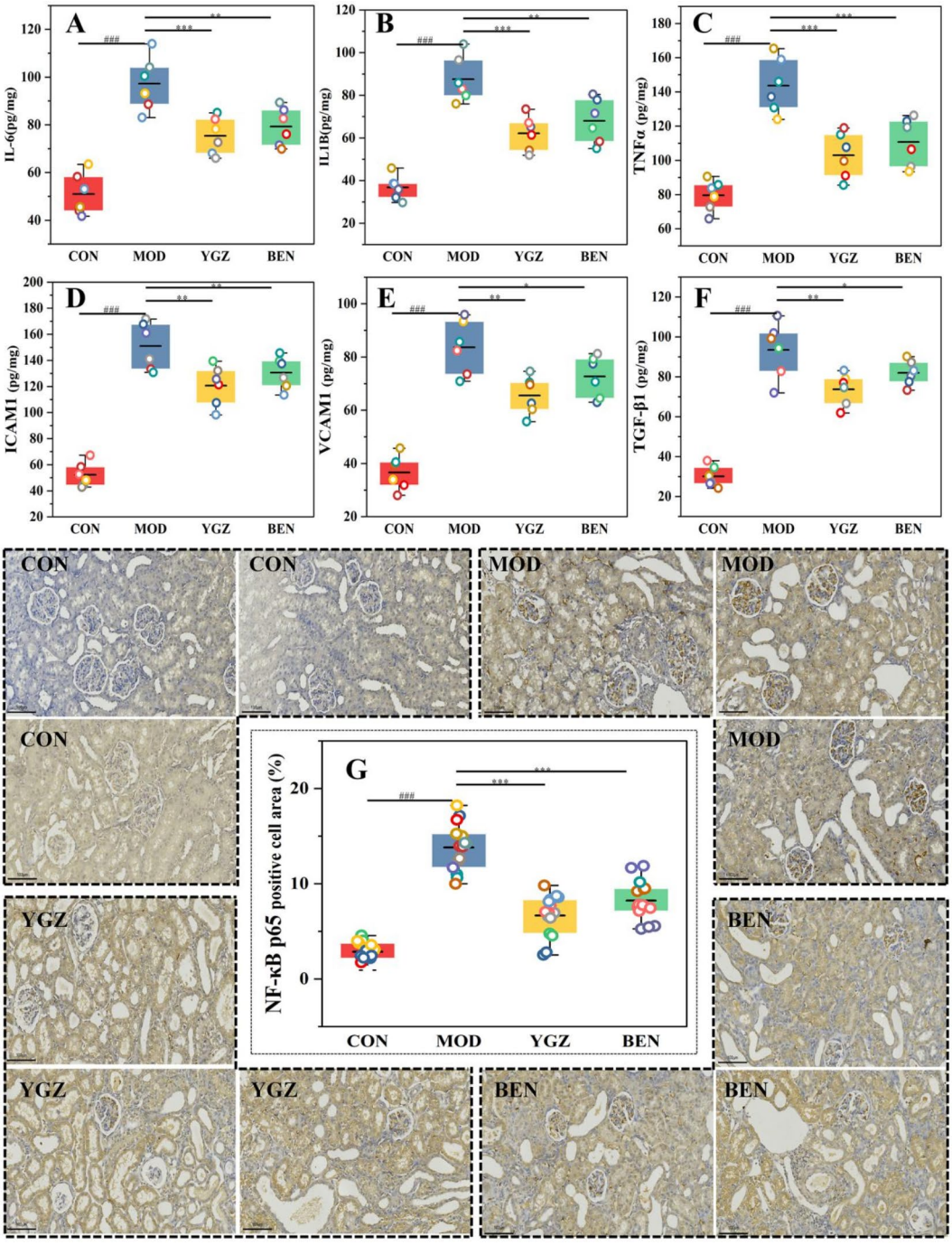

Fig. 5. Effects of YGZ on cytokines in kidney tissue. (**A**) IL-6, (**B**) IL-1B, (**C**) TNF-α, (**D**) ICAM-1, (**E**) VCAM-1, (**F**) TGF-β1, (**G**) immunohistochemical analysis of NF-κB p65 (200×, scale bar 100 μm) (Supplementary Table 7). Supplementation with YGZ extract significantly reduced the secretion of IL-6, IL-1β, TNF-α, ICAM-1, VCAM-1 and TGF-β1, attenuated the HUA-induced elevation of NF-κB p65 expression in the kidney. $^{###}p < 0.001$, $^{##}p < 0.01$, $^{#}p < 0.05$ vs. CON group. $^{***}p < 0.001$, $^{**}p < 0.01$, $^{*}p < 0.05$ vs. MOD group.

Network pharmacology analysis of YGZ anti-HUA/gout

Identification of active components and targets

A total of 109 components of YGZ were obtained from TCMSP and literature sources (Supplementary Table 9). After screening for ADME parameters, 36 components met the selection criteria. It is important to note that, though methyl caffeate (OB = 30.68%, DL = 0.06), ethyl gallate (OB = 25.61%, DL = 0.06), methyl gallate (OB = 30.91%, DL = 0.05), gallic acid (OB = 31.69%, DL = 0.04), protocatechuic acid (OB = 25.37, DL = 0.04) have a relatively low DL value, they are known to have good therapeutic effects, such as anti-hyperuricemia[22], anti-inflammation[24–27], anti-oxidant[28,29], anti-diabetic[30,31], and anti-atherosclerosis[32] properties. In consideration of

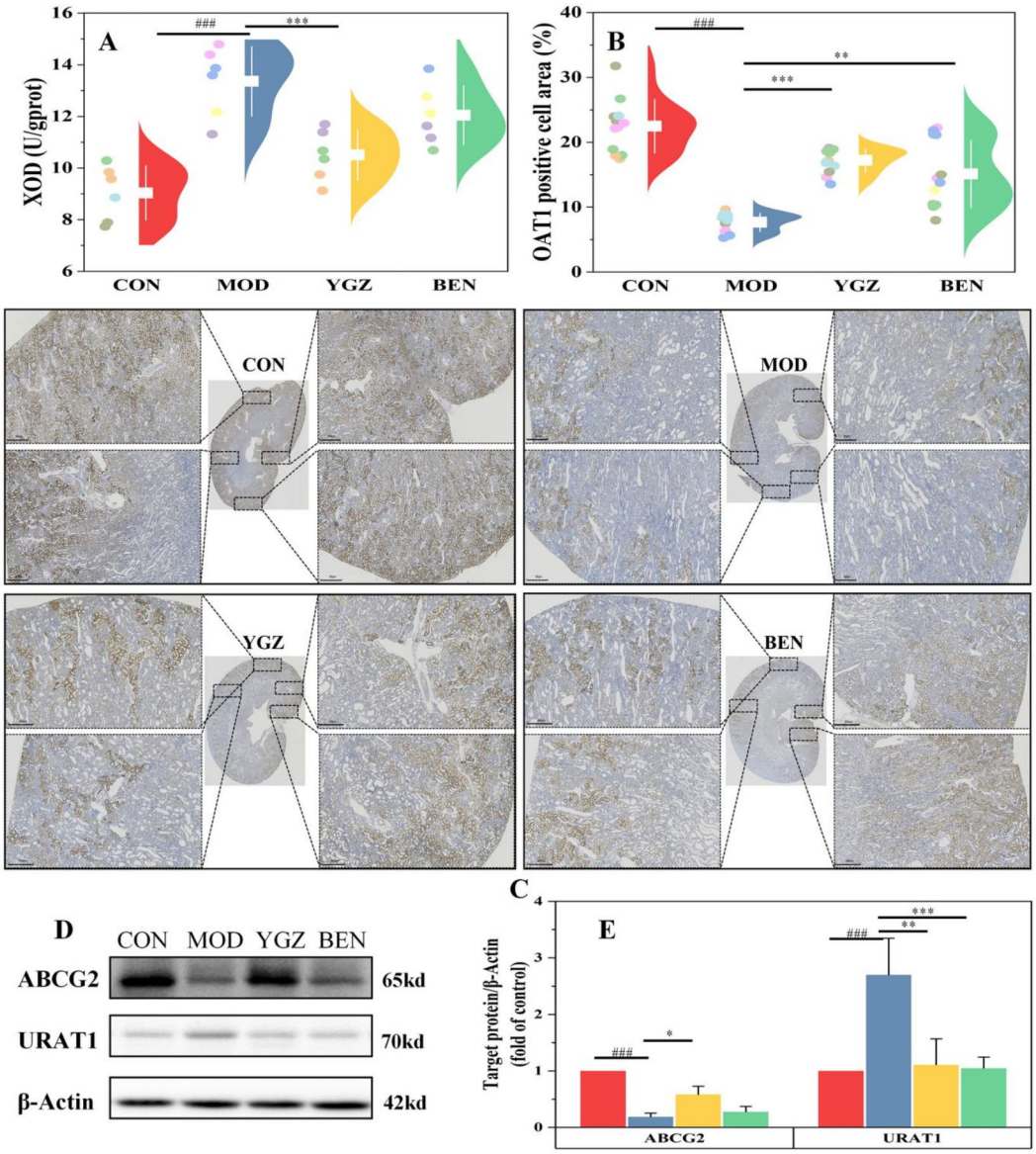

Fig. 6. Effects of YGZ on UA synthetase and UA transporters. (**A**) XOD activity, (**B**, **C**) immunohistochemical analysis of OAT1 (40×, scale bar 500 μm), (**D**, **E**) quantification of ABCG2 and URAT1 expression by Western blotting (Supplementary Table 8, original blots were presented in Supplementary Fig. 3). Supplementation with YGZ extract exhibits a significant inhibitory effect on XO activity, reverse the up-regulation of URAT1, and the down-regulation of ABCG2 and OAT1 in HUA rats. $^{###}p < 0.001$, $^{##}p < 0.01$, $^{#}p < 0.05$ vs. CON group. $^{***}p < 0.001$, $^{**}p < 0.01$, $^{*}p < 0.05$ vs. MOD group.

the potential pharmacological effects of these constituents, these 5 compounds were also included in subsequent analysis. Totally 41 components (including 18 organic acids, 14 flavonoids, 5 terpenoids, 2 steroids, 1 lignan, and 1 other common compound, Supplementary Table 9) of YGZ were selected as candidate components for further investigation. Furthermore, 539 targets interacting with the aforementioned 41 components were identified (Supplementary Table 10).

Shared targets between YGZ-related targets and HUA/gout-related Targets

Through a systematic review of the Genecard, DisGeNET and TTD databases, totally 363 HUA-related targets and 571 gout-related targets were identified (Supplementary Table 11). A total of 138 shared targets among YGZ-related targets, HUA-related targets and gout-related targets were identified as therapeutic targets of YGZ against HUA and gout.

C-T network, PPI network construction and analysis

As illustrated in Fig. 7A, the C-T network was composed of 580 nodes (including 41 component nodes and 539 target nodes) and 1953 edges. Based on the shared targets among YGZ-related targets and HUA/gout-

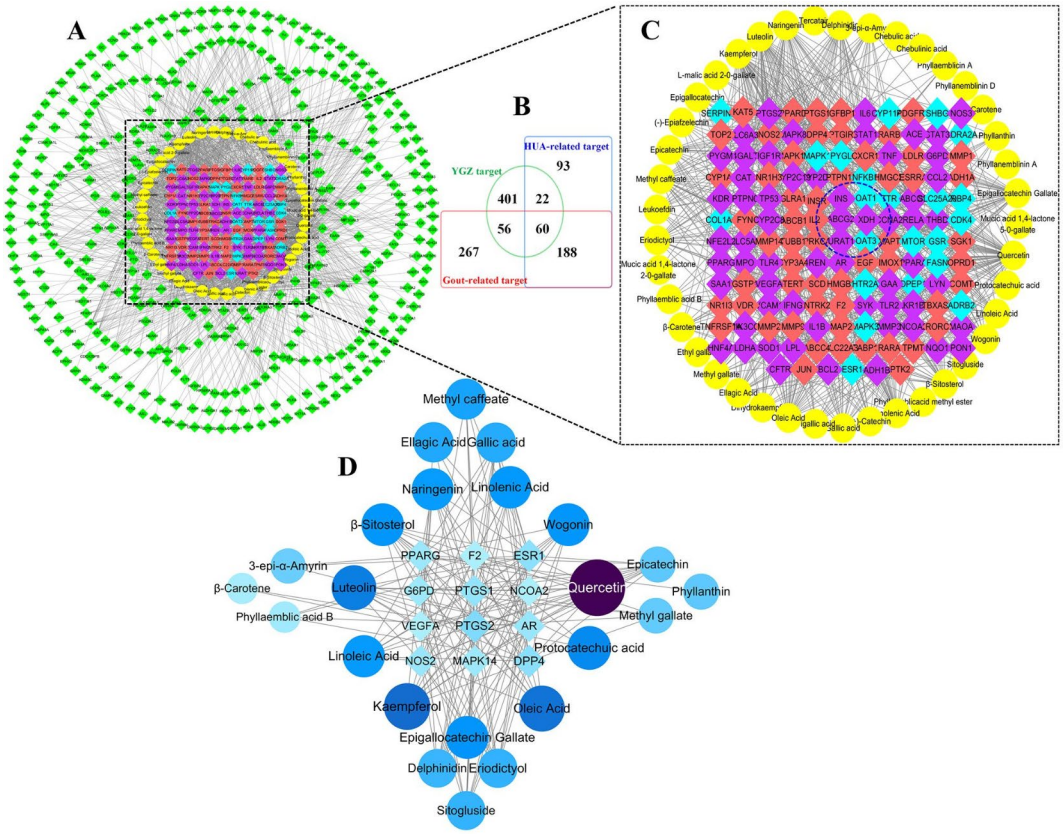

Fig. 7. Component-target network of YGZ. (**A**) C-T network of YGZ, (**B**) Venn diagram among YGZ-related targets, HUA-related targets, and gout-related targets, (**C**) potential C-T network of YGZ in treating HUA and gout, (**D**) Hub C-T network of YGZ in treating HUA and gout.

related targets (Fig. 7B), 41 components and 138 potential therapeutic targets were selected to construct the potential C-T network of YGZ against HUA/gout (Fig. 7C). By conducting network analysis using the screening criteria of DC ≥ median DC, BC ≥ median BC, and CC ≥ median CC, 23 compounds, including quercetin, kaempferol, luteolin, oleic acid, epigallocatechin gallate, naringenin, β-sitosterol, linolenic acid, delphinidin, wogonin, methyl caffeate, sitogluside, gallic acid, ellagic acid, linoleic acid, eriodictyol, epicatechin, 3-epi-α-Amyrin, methyl gallate, protocatechuic acid, β-carotene, phyllanthin, and phyllaemblic acid B were identified as the significant bioactive components in YGZ (Fig. 7D).

To further reveal the action mechanism of YGZ's therapeutic targets, a PPI network of 138 potential targets was constructed (Fig. 8A). Four topological parameters, including MCC, DC, BC and CC were employed to assess the centrality of these nodes. The top 30 nodes for each criterion were displayed. Sixteen hub gens, including IL6, STAT3, TNF, IL1B, JUN, MAPK3, TLR4, BCL2, PTGS2, MMP9, TP53, INS, MAPK8, ESR1, PPARG and MTOR, were selected for simultaneously possessing high MCC, DC, BC and CC values (Fig. 8B). These genes were primarily involved in the positive regulation of gene expression, transcription from RNA polymerase II promoter, apoptotic process and inflammatory response (Fig. 8C). The top 10 enriched pathways of these 16 hub genes were mainly associated with lipid and atherosclerosis, endocrine resistance, TH17 cell differentiation, pathways in cancer, IL-17, AGE-RAGE, TNF, TLRS, HIF-1 and NOD-like receptor signaling pathway (Fig. 8D).

In comparison to the C-T network of the three clinical drugs (including allopurinol, febuxostat and benzbromarone) for hyperuricemia (as illustrated in Supplementary Fig. 2), YGZ demonstrated a greater number of therapeutic advantages due to its "multicomponents-multitarget" characteristic. In addition to targeting uric acid-producing enzyme (XDH) and uric acid transporters (URAT1, OAT1, ABCG2, OAT3, etc.) to inhibit uric acid production and promote uric acid excretion, YGZ also regulated target proteins on the glycolipid metabolic pathway, inflammatory pathway, and insulin resistance pathway. By targeting these various pathways, YGZ represents a promising natural alternative or adjunct therapy for the management of hyperuricemia and its associated comorbidities.

GO and KEGG pathway enrichment analysis

As demonstrated in Fig. 9A, YGZ anti-HUA targets were significantly enriched in various modules, including response to purine-containing compound, tumor necrosis factor, lipopolysaccharide, oxidative stress, regulation of lipid metabolic process, inflammatory response, IL-8 production, and PI3K signaling. Meanwhile, the GO terms of YGZ-anti gout targets were primarily associated with the regulation of lipid metabolic processes, IL-6

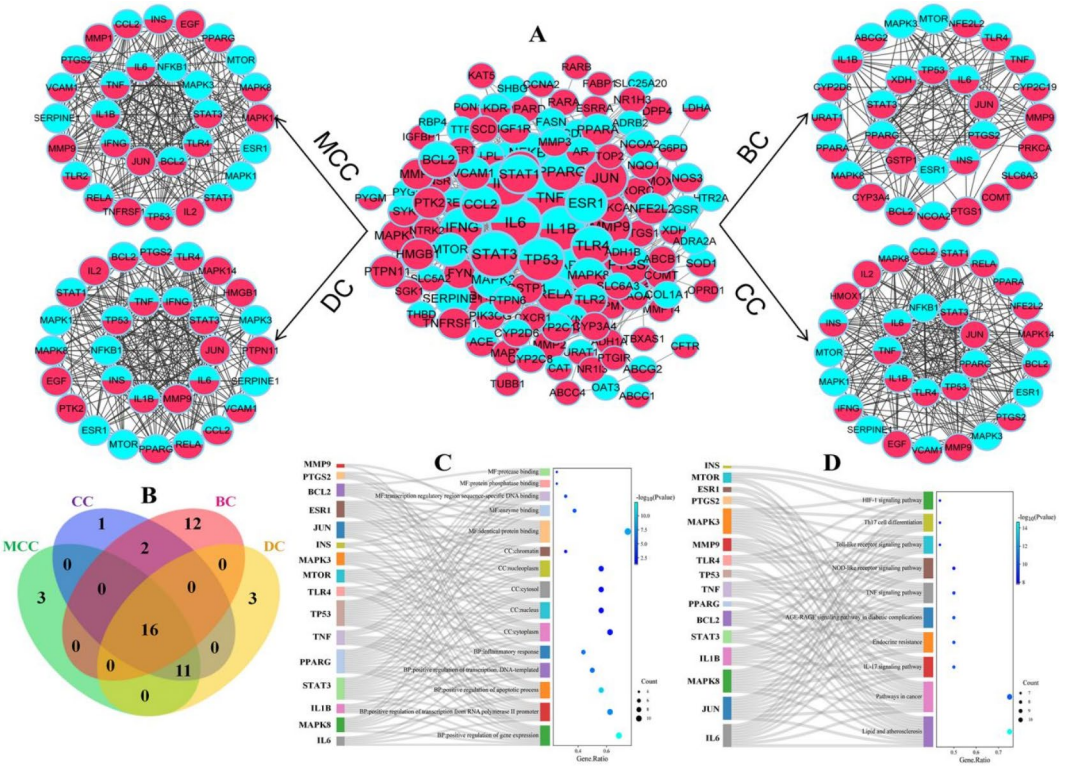

Fig. 8. PPI network and analysis. (**A**) PPI network of shared targets among YGZ, HUA and gout-related targets, (**B**) Hub PPI network, (**C**) GO enrichment analysis for 16 hub targets, (**D**) KEGG enrichment analysis for 16 hub targets.

production, extrinsic apoptotic signaling, smooth of muscle cell proliferation, response to alcohol, xenobiotic stimulus, chemical stress, and epithelial cell migration (Fig. 9B).

The KEGG functional enrichment analysis indicated that YGZ exerts a significant influence on a multitude of signaling pathways in HUA and gout, including AGE-RAGE signaling pathway in diabetic complications, lipid and atherosclerosis, fluid shear stress and atherosclerosis, insulin resistance, rheumatoid arthritis, HIF-1, PI3K-Akt, TNF, IL-17, TLRS, MAPK, and NF-κB signaling pathways (Fig. 9C,D).

Integrated network construction

To elucidate the potential mechanisms of YGZ in treating HUA and gout, a network of "component-target-pathway" was constructed, based on 23 core bioactive components, 25 hub targets and 12 KEGG pathways (Fig. 10). The therapeutic effects of YGZ against HUA and gout are exerted through multiple targets affecting diverse pathways, including anti-inflammatory, insulin resistance improvement, and glucolipid metabolism amelioration. These effects are attributed to the diverse bioactive components present in YGZ, including organic acids (gallic acid, ellagic acid, methyl gallate, protocatechuic acid, etc.), flavonoids (quercetin, kaempferol, luteolin, epigallocatechin gallate, naringenin, delphinidin, etc.), terpenoids (3-epi-α-Amyrin, β-Carotene, phyllaemblic acid B), and steroids (β-Sitosterol, Sitogluside).

Molecular docking analysis

A heatmap of docking scores between active components and critical targets was presented in Fig. 11A. The lower docking score, the stronger binding affinity. Especially, the docking score of methyl caffeate-XDH, quercetin-ABCG2, epicatechin-URAT1, phyllaemblic acid B-OAT1, kaempferol-IRS1, ellagic Acid-MAPK3, eriodictyol-MMP9, epigallocatechin gallate-MTOR, luteolin-PTGS2, gallic acid-TLR4, luteolin-PPARG, gallic acid-TP53, epigallocatechin gallate-MAPK14, epigallocatechin gallate-ESR1, and other 109 compound-target interactions were all less than -7.00, implying strong bindings. The stable compoment-target complexes are presented and visually displayed in Fig. 11B. The active components are primarily formed by hydrogen bonds, Pi-Pi stacking, and Pi-cation interactions with the amino acid residues of the targets. For instance, XDH's amino acid residues GLU 802, ARG 880, and THR 1010 formed hydrogen bond interactions with methyl caffeate. ABCG2's amino acid residues PHE 439 formed Pi-Pi stacking with quercetin. MTOR's amino acid residues ARG 73 formed Pi-cation interaction with epigallocatechin gallate.

Molecular dynamics simulations analysis

In the present study, URAT1, which is regarded as the most significant transporter in regulating uric acid homeostasis, was selected for further analysis of the stability of binding to epicatechin, ellagic acid, and

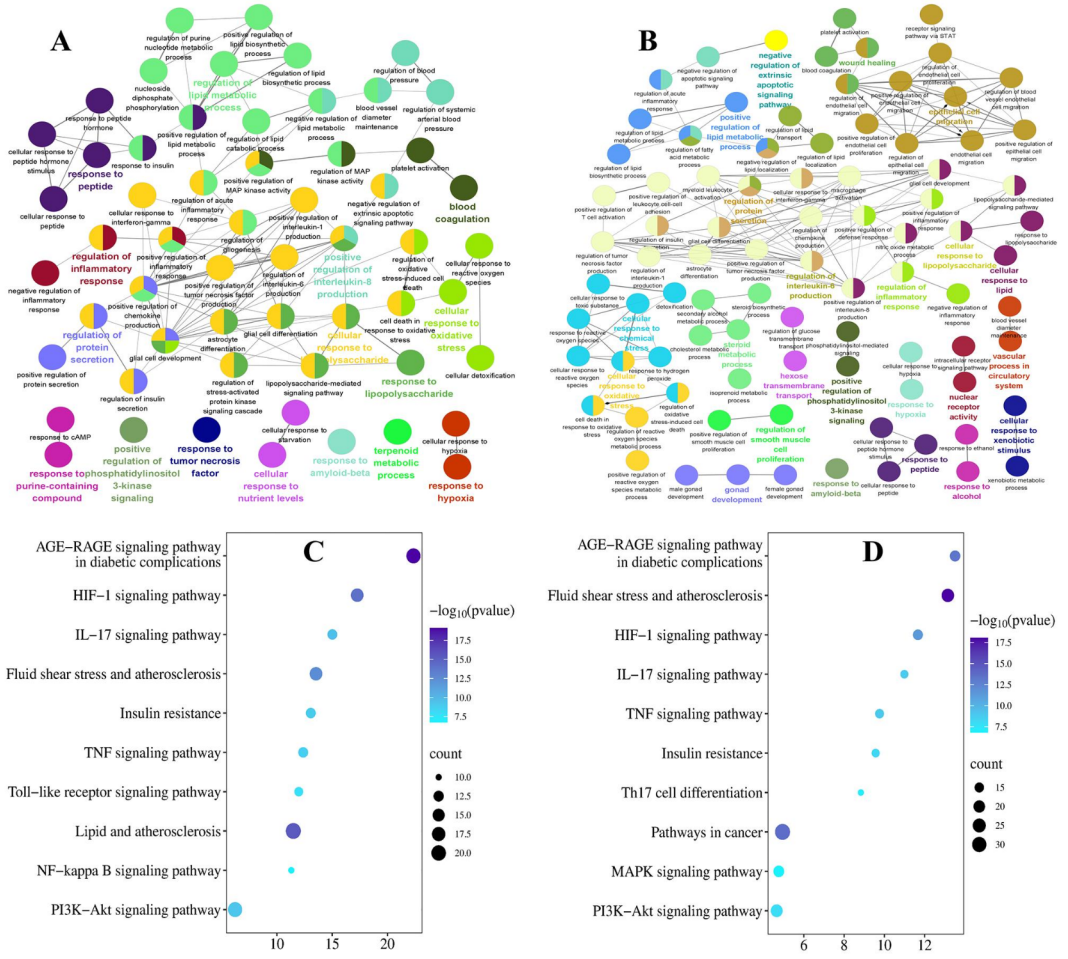

Fig. 9. GO and KEGG enrichment analysis. (**A**) GO enrichment analysis for YGZ anti-HUA targets, (**B**) GO enrichment analysis for YGZ anti-gout targets, (**C**) KEGG enrichment analysis for YGZ anti-HUA targets, (D) KEGG enrichment analysis for YGZ anti-gout targets.

epigallocatechin gallate. As illustrated in Fig. 12A, all three complexes attained stability at the conclusion of the simulation, exhibiting root-mean-square deviations (RMSDs) of approximately 0.45 nm. The subsequent RMSF analysis (Fig. 12B) revealed relatively low values (between 0.1 and 0.5 nm) for the three protein complexes, indicating less residue fluctuation and stronger binding. The stable gyration radius (Rg) values of these systems exhibited fluctuations between 2.70 nm and 2.95 nm (Fig. 12C), indicating the stability of the protein structure. It was noteworthy that the epigallocatechin gallate-URAT1 complex exhibited a relatively higher number of hydrogen bonds compared to the other two complex systems, indicating a more stable and compact structure in their binding (Fig. 12D). Epigallocatechin gallate interacted with the residues MET 214, ASN 237, SER 238, GLY 446, THR 450, and GLN 473, thereby stabilizing the complex (Fig. 12E,F). The total binding free energy was calculated via MM/PBSA methods, yielding -24.55 ± 3.41 kcal/mol for epicatechin-URAT1, -21.84 ± 3.76 kcal/mol for ellagic acid-URAT1, and -45.57 ± 7.43 kcal/mol for epigallocatechin gallate-URAT1, respectively. These findings underscore the importance of epigallocatechin gallate in targeted URAT1 for HUA and gout.

Discussion

Hyperuricemia has emerged as a significant public health concern worldwide, affecting an estimated 14% in China, up to 20% in the USA, and varying in prevalence across countries[4,33]. Although HUA is typically asymptomatic, evidence from basic science suggests that it plays a contributing role in the pathogenesis of gout, metabolic syndrome, nephropathy, and cardiovascular diseases, through the induction of inflammation, insulin resistance, endothelial dysfunction, and the activation of renin-angiotensin system. Consequently, a comprehensive and long-term management is essential upon diagnosis. The serum UA pool is maintained in equilibrium by the coordinated actions of UA production and excretion. When UA production exceeds its excretion, HUA ensues. HUA is classified into three types based on the underlying etiological factors: UA overproduction type (accounting for about 10%), UA underexcretion type (60%), and combined type (30%)[34]. Although XO inhibitors remain the primary treatment for HUA and gout, it is crucial to recognize that serum UA regulation is primarily determined by UA excretion, which is achieved through the urate transporters located in the renal tubule, including URAT1, GLUT9, ABCG2, OAT1, OAT3, OAT4, NPT1, and others[8,35].

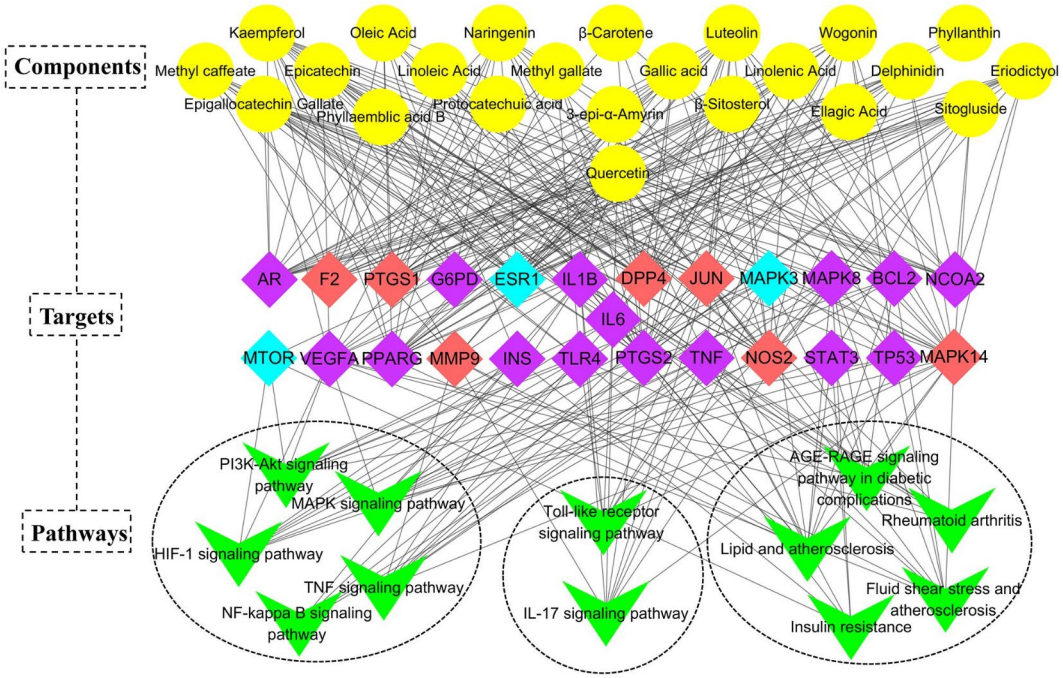

Fig. 10. "Component-target-pathway" network of YGZ in treating HUA and gout.

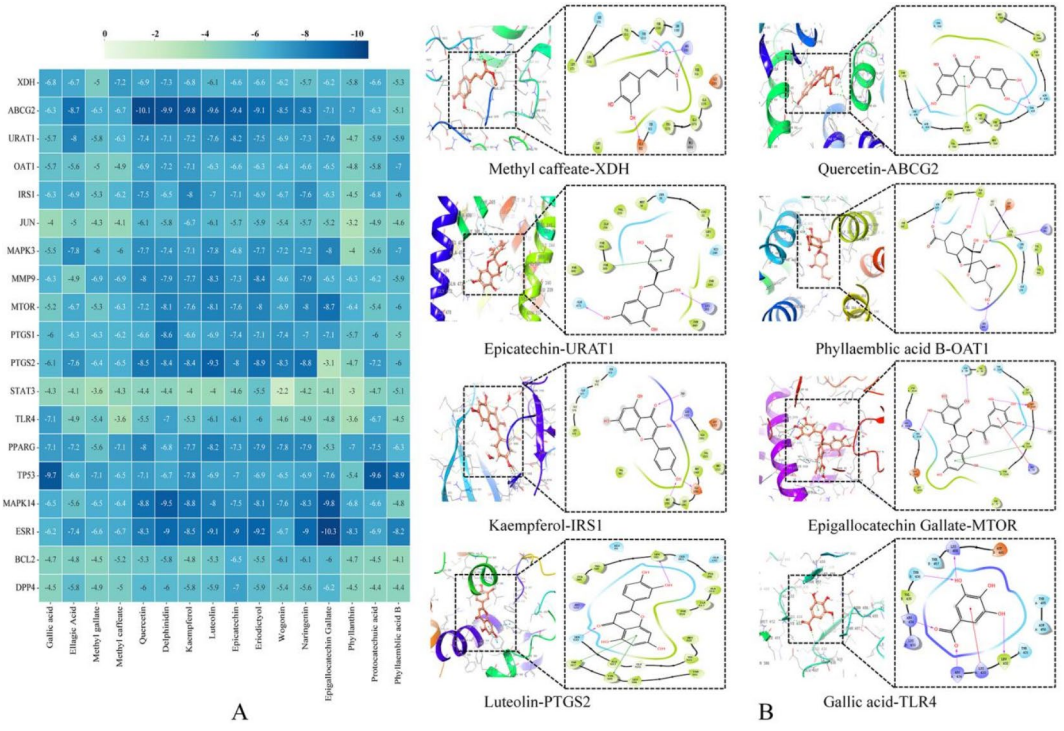

Fig. 11. Molecular docking analysis of active compounds and target proteins. (**A**) Heatmaps of docking score, (**B**) Molecular docking models of active compounds interacting with target proteins in 3D and 2D diagrams.

In this study, urate transporter expression, as well as XO activity, cytokine levels and histopathological changes were simultaneously assessed to elucidate the anti-HUA efficacy and mechanism of YGZ. Encouragingly, supplementation with YGZ markedly inhibited the UA synthesis via suppressing the XO activity, and promoted UA excretion by up-regulating of OAT1 and ABCG2, while down-regulating of URAT1. Furthermore, YGZ

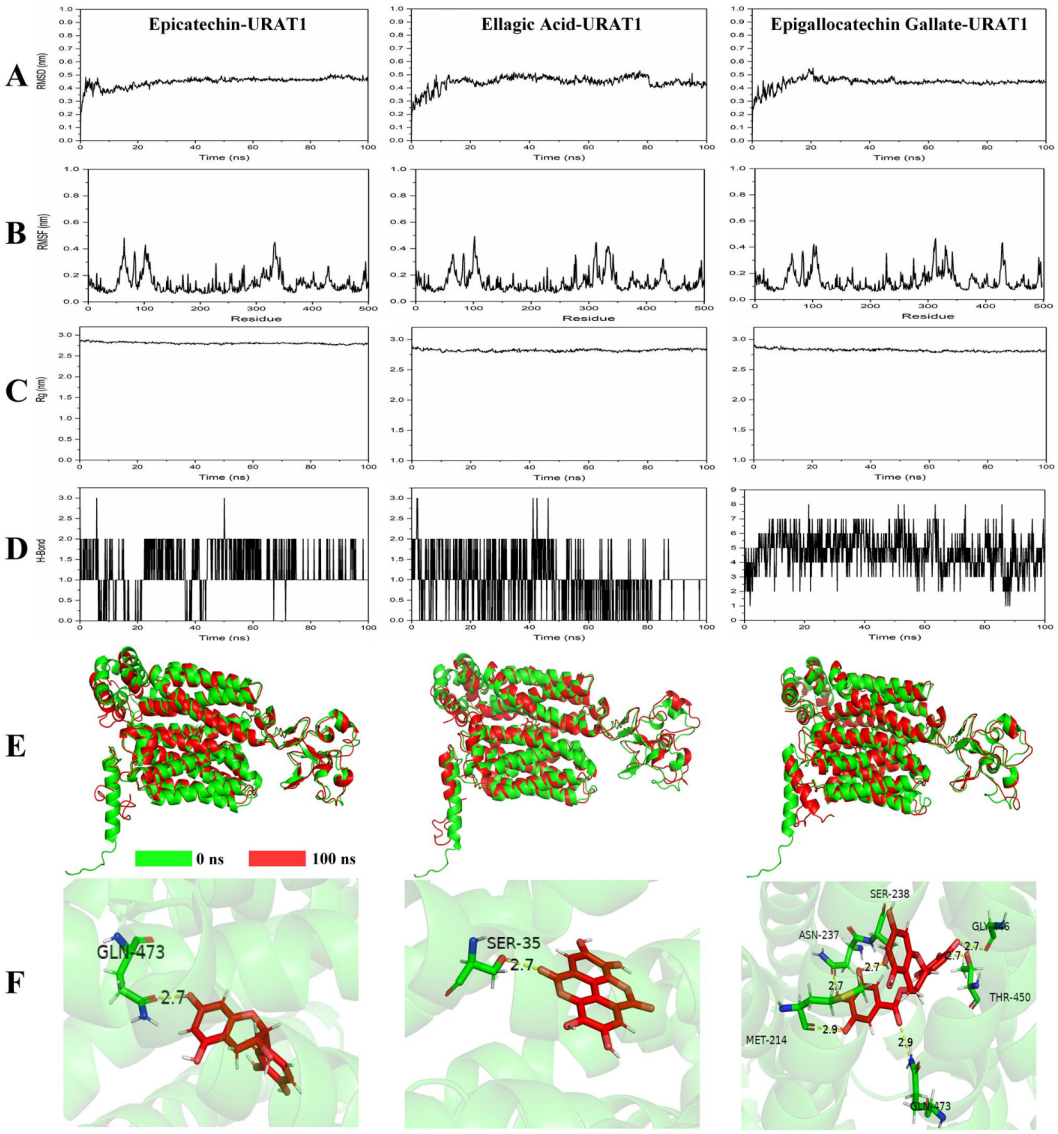

Fig. 12. The molecular dynamics simulation results of epicatechin-URAT1, ellagic acid-URAT1, and epigallocatechin gallate-URAT1. (**A**) the RMSD of three complexes, (**B**) the RMSF of three complexes, (**C**) the Rg of three complexes, (**D**) the H-bonds of three complexes, (**E**) structures of three complexes before and after simulation, and (**F**) the binding mode of three complexes after simulation.

administration improved abnormal glucolipid metabolism, enhanced antioxidant capacity, and suppressed the secretion and protein expression of cytokines.

XO is the key enzyme responsible for catalysing the oxidation process of hypoxanthine into xanthine and ultimately into UA. Inhibiting XO represent the most common strategy employed in treating HUA and gout. A multitude of compounds derived from food plants possess the optimal structural characteristics essential for XO inhibition, including flexible backbone, hydrogen bond acceptors and donors, and hydrophobic nature. Such compounds are generally recognized as being much safer than existing drugs such as allopurinol[36,37]. YGZ contains a number of active ingredients, including gallic acid, ellagic acid, quercetin, and kaempferol, which have lower docking scores and demonstrate more potent XO inhibitory activity[37–40]. These findings are consistent with the previously cited research.

In the pathogenesis of HUA, reduced renal excretion of UA plays a more prominent role. As a sophisticated transport mechanism, UA excretion is the consequence of the coordinated activity of multiple genes. It is postulated that an integrated multi-target pharmaceutical intervention strategy would be more efficacious in regulating the disease network than a single-targeting molecule with a strong-affinity ligand[41]. URAT1, situated at the apical membrane of the proximal renal tubule, is a crucial carrier responsible for UA reabsorption. OAT1, located at the basolateral side of proximal renal tubules, plays a pivotal role in the excretion of UA via transporting UA from the renal interstitial into renal proximal tubule epithelial cells[34]. ABCG2, situated at the apical surface of proximal tubule cells and enterocytes, is involved in the export of UA in both kidney and intestine. It has been demonstrated that dysfunctional variants of ABCG2 are associated with elevated serum

uric acid levels and a heightened risk of gout[8,42]. Protein analysis indicated that supplementation of YGZ can significantly diminish the reabsorption of UA by reducing the expression of renal URAT1, while enhancing its excretion through the increase in the expression of renal OAT1 and ABCG2. Molecular docking results indicate that ellagic acid, quercetin, delphinidin, kaempferol, luteolin, epicatechin, eriodictyol, wogonin, naringenin, epigallocatechin gallate, and phyllanthin exhibit excellent binding activity to URAT1, OAT1, and ABCG2. Quercetin has been identified as an active ingredient responsible for inhibiting URAT1 with a small IC50 value of 12.6 μM[43]. Moreover, it has been demonstrated to inhibit the downregulation of OAT1[44]. Naringenin was found to enhance the expression of ABCG2 by increasing the abundance of PDZK1 in both in vivo and in vitro settings[45]. Epigallocatechin gallate exerts anti-hyperuricemia effects via the promotion of OAT1 expression and the inhibition of URAT1 expression[46]. The organic acids and flavonoids present in YGZ may be the principal active components in the regulation of urate transporters.

A persistently elevated serum UA level has been associated with the pathogenesis of renal inflammatory and fibrosis[47]. Recent research findings suggested that both urate crystals and soluble UA can trigger inflammatory pathways, ultimately inducing the expression or release of cytokines (e.g. IL6, IL1B, TNFα, TGFβ1, PGE2), and adhesion molecules (e.g. VCAM1, ICAM1), which in turn stimulate TLR4/MyD88/NLRP3/NF-κB pathways[4,48]. Furthermore, serum UA activates the TGF-β1/Smad, NF-κB, and Erk signaling pathways in renal tubules, resulting in the secretion of inflammatory cells and subsequent macrophage migration. Elevated levels of UA impede the phosphorylation of signal transducer and activator of STAT3, thereby inducing apoptosis in both in vivo and in vitro[49]. Therapies that lower UA levels and those targeting various aspects of the immune system have been demonstrated to be beneficial for HUA and related complications. The present study demonstrated that YGZ administration effectively alleviated inflammation in HUA rats by decreasing the secretion of IL1B, IL6, TNFα, ICAM1, VCAM1, and TGFβ1, along with the expression of NF-κB p65 in kidney. Moreover, the network pharmacological analysis indicated that YGZ exerted its effects on STAT1, IL1B, MAPK14, TNF, TLR4, RELA, TLR2, JUN, VCAM1, PTGS2, TNF, RELA, NFKB1, TNFRSF1A, IL6, MAPK8, CCL2, IFNG, and medicated the Th17 cell differentiation, T cell receptor, TLRs, NF-κB, TNF, IL-17, NOD-like receptor signaling pathway, thus exerting anti-inflammatory and nephroprotective effects. Certain active components of YGZ have been reported to possess anti-inflammatory properties. Gallic acid, as a dietary polyphenol substance with potent antioxidant activity, is the main bioactive component in YGZ. It modulates the inflammatory response by regulating several signaling pathways, including JAK-STAT, cytokine receptor, TLR4/NF-κB, and NOD-like receptor, involving STAT1, NFKB1, RELA, COX-2, VEGF and TNF-α[50,51]. Ellagic acid notably reduces the levels of COX-2 and TNF-α, as well as suppresses the protein synthesis of NF-κB[52]. Luteolin suppresses the protein expression of NLRP3, ASC, CASP1, IL-18, and IL-1β, thereby inhibiting the activation of NLRP3 inflammasomes[53]. Epigallocatechin gallate significantly decreases the expression of IL6, IL1B, TNFα, TLR4, and iNOS, suppresses IκB and p65 phosphorylation, thereby inhibiting the activation of the NF-κB pathway[54]. Delphinidin inhibites the expression of iNOS, NO, IL6, and TNFα. Moreover, it down-regulates the activity of NF-κB and MEK1/2-ERK1/2 signaling pathways for anti-inflammatory purposes[55].

Epidemiological data indicates that premenopausal women have lower incidence of HUA than men. Elevated serum UA levels in post-menopausal women are strongly correlated with female hormone loss[56,57]. Takiue et al. conducted a research to investigate the female hormone-related regulation of renal urate transporter expression in ovariectomized mice. The result demonstrated that estradiol can significantly suppress the protein expression of URAT1 and GLUT9[58]. Additionally, estrogen can modulate the activities of xanthine dehydrogenase (XDH) and xanthine oxidase (XO) through a receptor-independent mechanism[59]. In Ayurvedic medicine, YGZ has been traditionally employed to treat menorrhagia and enhance female fertility, due to its robust estrogenic and follicle-stimulating hormone-like activity[60]. In present network pharmacology research, ESR1 is identified as a pivotal target within the hub C-T network (Fig. 7D), which is demonstrably linked to serum estrogen levels[61]. It is possible that YGZ may regulate the hormone levels by acting on ESR1 to inhibit UA production and promote UA excretion. This may provide new insight into the therapeutic efficacy of YGZ in treating HUA. Moreover, estrogens, through their receptors ESR1 and ESR2, play a crucial role in metabolic regulation, including glucose and lipid metabolism, as well as insulin sensitivity[62,63]. It provide a new focus on the potential of YGZ in treating other metabolic disorders.

Conclusion

In conclusion, the therapeutic effect and potential mechanism of YGZ against HUA and gout were investigated in present study through integrating pharmacological experimentation, network pharmacology, and molecular docking studies. YGZ exerts pronounced therapeutic effects against HUA through a number of mechanisms, including the promotion of UA excretion, inhibition of UA production, amelioration of disorder of glucolipid metabolism, and the provision of antioxidant and anti-inflammatory properties. The regulatory effect of YGZ on urate transporters in the kidney was first investigated, thereby further expanding the scientific connotation of YGZ in promoting UA excretion. Organic acids and flavonoids, as the principal active components of YGZ, regulate the disease network via lipid and atherosclerosis, fluid shear stress and atherosclerosis, rheumatoid arthritis, insulin resistance, HIF-1, PI3K-Akt, TNF, IL-17, TLRS, MAPK, and NF-κB signaling pathways, thereby treating HUA and gout. These findings provide evidence of the therapeutic potential of YGZ and establish a robust theoretical foundation for the development of natural foods derived from YGZ to alleviate HUA. Furthermore, it should be noted that the therapeutic efficacy of the aforementioned components should be validated through in vitro or in vivo experiments in the future.

Data availability

Raw data for this study can be obtained by contacting the corresponding author.

Received: 1 July 2024; Accepted: 8 November 2024
Published online: 11 November 2024

References

1. Piao, W. et al. The prevalence of hyperuricemia and its correlates among adults in China: Results from CNHS 2015–2017. *Nutrients* **14**(19), 4095 (2022).
2. Kuo, C. F., Grainge, M. J., Mallen, C., Zhang, W. & Doherty, M. Rising burden of gout in the UK but continuing suboptimal management: a nationwide population study. *Ann. Rheum. Dis.* **74**(4), 661–667 (2015).
3. Türker, P. F., Hoca, M., Özduran, G., Akçil Ok, M. & DemirÇelebi, M. The correlation of uric acid levels with biochemical parameters and dietary factors in individuals with asymptomatic hyperuricemia and gouty arthritis. *Nucleosides Nucleotides Nucl. Acids* **41**(5–6), 444–462 (2022).
4. Joosten, L. A. B., Crişan, T. O., Bjornstad, P. & Johnson, R. J. Asymptomatic hyperuricaemia: A silent activator of the innate immune system. *Nat. Rev. Rheumatol.* **16**(2), 75–86 (2020).
5. Johnson, R. J. et al. Hyperuricemia, acute and chronic kidney disease, hypertension, and cardiovascular disease: Report of a scientific workshop organized by the national kidney foundation. *Am. J. Kidney Dis.* **71**(6), 851–865 (2018).
6. Lee, S. C., Wo, W. K., Yeoh, H. S., Mohamed Ali, N. & Hariraj, V. Allopurinol-induced severe cutaneous adverse drug reactions: An analysis of spontaneous reports in Malaysia (2000–2018). *Ther. Innov. Regul. Sci.* **55**(3), 514–522 (2021).
7. Wang, M. et al. The major cardiovascular events of febuxostat versus allopurinol in treating gout or asymptomatic hyperuricemia: A systematic review and meta-analysis. *Ann. Palliat. Med.*. **10**(10), 10327–10337 (2021).
8. Dalbeth, N. et al. Gout. Nature reviews. *Dis. Prim.* **5**(1), 69 (2019).
9. Prananda, A. T. et al. *Phyllanthus emblica*: A comprehensive review of its phytochemical composition and pharmacological properties. *Front. Pharmacol.* **14**, 1288618 (2023).
10. Li, G. et al. Phyllanthi Fructus: A modal medicinal and food homologous item in quality evaluation. *Chin. Herbal Med.*. **15**(3), 360–368 (2023).
11 Fatima, N., Pingali, U. & Muralidhar, N. Study of pharmacodynamic interaction of *Phyllanthus emblica* extract with clopidogrel and ecosprin in patients with type II diabetes mellitus. *Phytomed. Int. J. Phytother. Phytopharmacol.* **21**(5), 579–585 (2014).
12. Luo, X. et al. *Phyllanthus emblica* aqueous extract retards hepatic steatosis and fibrosis in NAFLD mice in association with the reshaping of intestinal microecology. *Front. Pharmacol.* **13**, 893561 (2022).
13. Huang, S. M., Lin, C. H., Chang, W. F. & Shih, C. C. Antidiabetic and antihyperlipidemic activities of *Phyllanthus emblica* L. extract in vitro and the regulation of Akt phosphorylation, gluconeogenesis, and peroxisome proliferator-activated receptor α in streptozotocin-induced diabetic mice. *Food Nutr. Res.* https://doi.org/10.29219/fnr.v67.9854 (2023).
14. Sharif, M. A. et al. *Phyllanthus emblica* (Amla) methanolic extract regulates multiple checkpoints in 15-lipoxygenase mediated inflammopathies: Computational simulation and in vitro evidence. *Saudi Pharm. J. SPJ Off. Publ. Saudi Pharm. Soc.* **31**(8), 101681 (2023).
15. Zhao, T., Sun, Q., Marques, M. & Witcher, M. Anticancer properties of *Phyllanthus emblica* (Indian Gooseberry). *Oxid. Med. Cell. Longev.* **2015**, 950890 (2015).
16 Tao, H., Zhong, J., Mo, Y., Liu, W. & Wang, H. Exploring the mechanism through which *Phyllanthus emblica* L. extract exerts protective effects against acute gouty arthritis: A network pharmacology study and experimental validation. *Evidence-Based Complement. Alternat. Med. eCAM.* **2022**, 9748338 (2022).
17. Sarvaiya, V. N. et al. Evaluation of antigout activity of *Phyllanthus emblica* fruit extracts on potassium oxonate-induced gout rat model. *Vet. World.* **8**(10), 1230–1236 (2015).
18. Gong, M. et al. Effect of Eucommia ulmoides leaves on hyperuricemia and kidney injury induced by a high-fat/high-fructose diet in rats. *Iran. J. Basic Med. Sci.* **25**(4), 527–535 (2022).
19. Yustisia, I., Tandiari, D., Cangara, M. H., Hamid, F. & Daud, N. A. A high-fat, high-fructose diet induced hepatic steatosis, renal lesions, dyslipidemia, and hyperuricemia in non-obese rats. *Heliyon.* **8**(10), e10896 (2022).
20. Shan, B., Chen, T., Huang, B., Liu, Y. & Chen, J. Untargeted metabolomics reveal the therapeutic effects of Ermiao wan categorized formulas on rats with hyperuricemia. *J. Ethnopharmacol.* **281**, 114545 (2021).
21. Cui, J. et al. Chloroquine inhibits NLRP3 inflammasomes activation and alleviates renal fibrosis in mouse model of hyperuricemic nephropathy with aggravation by a high-fat-diet. *Int. Immunopharmacol.* **120**, 110353 (2023).
22. Kanehisa, M. & Goto, S. KEGG: Kyoto encyclopedia of genes and genomes. *Nucl. Acids Res.* **28**, 27–30 (2000).
23. Kanehisa, M., Furumichi, M., Sato, Y., Kawashima, M. & Ishiguro-Watanabe, M. KEGG for taxonomy-based analysis of pathways and genomes. *Nucl. Acids Res.* **51**, D587–D592 (2023).
24. Park, P. H., Hur, J., Kim, Y. C., An, R. B. & Sohn, D. H. Involvement of heme oxygenase-1 induction in inhibitory effect of ethyl gallate isolated from Galla Rhois on nitric oxide production in RAW 264.7 macrophages. *Arch. Pharm. Res.* **34**(9), 1545–1552 (2011).
25. Mehla, K., Balwani, S., Agrawal, A. & Ghosh, B. Ethyl gallate attenuates acute lung injury through Nrf2 signaling. *Biochimie.* **95**(12), 2404–2414 (2013).
26. Zhou, P. et al. Methyl gallate alleviates acute ulcerative colitis by modulating gut microbiota and inhibiting TLR4/NF-κB pathway. *Int. J. Mol. Sci.* **23**(22), 14024 (2022).
27. Salama, A. A. A., Elgohary, R. & Fahmy, M. I. Protocatechuic acid ameliorates lipopolysaccharide-induced kidney damage in mice via downregulation of TLR-4-mediated IKBKB/NF-κB and MAPK/Erk signaling pathways. *J. Appl. Toxicol. JAT.* **43**(8), 1119–1129 (2023).
28 Choi, M. H., Yang, S. H., Kim, D. S., Kim, N. D. & Shin, H. J. Ethyl gallate isolated from *Castanopsis cuspidata* var. sieboldii branches inhibits melanogenesis and promotes autophagy in B16F10 cells. *Antioxidants.* **12**(2), 269 (2023).
29. Li, Y. et al. Methyl gallate prevents oxidative stress induced apoptosis and ECM degradation in chondrocytes via restoring Sirt3 mediated autophagy and ameliorates osteoarthritis progression. *Int. Immunopharmacol.* **114**, 109489 (2023).
30 Lee, D. et al. Methyl caffeate isolated from the flowers of *Prunus persica* (L.) batsch enhances glucose-stimulated insulin secretion. *Biomolecules.* **11**(2), 279 (2021).
31. Ahn, D. et al. Ethyl gallate dual-targeting PTPN6 and PPARγ shows anti-diabetic and anti-obese effects. *Int. J. Mol. Sci.* **23**(9), 5020 (2022).
32. Liu, W. et al. The benzoate plant metabolite ethyl gallate prevents cellular- and vascular-lipid accumulation in experimental models of atherosclerosis. *Biochem. Biophys. Res. Commun.* **556**, 65–71 (2021).
33. Zhang, M. et al. Prevalence of hyperuricemia among Chinese adults: Findings from two nationally representative cross-sectional surveys in 2015–2016 and 2018–2019. *Front. Immunol.* **12**, 791983 (2022).
34. Yanai, H., Adachi, H., Hakoshima, M. & Katsuyama, H. Molecular biological and clinical understanding of the pathophysiology and treatments of hyperuricemia and its association with metabolic syndrome, cardiovascular diseases and chronic kidney disease. *Int. J. Mol. Sci.* **22**(17), 9221 (2021).
35. Köttgen, A. et al. Genome-wide association analyses identify 18 new loci associated with serum urate concentrations. *Nat. Genet.* **45**(2), 145–154 (2013).
36. Yuan, M. et al. The interaction of dietary flavonoids with xanthine oxidase in vitro: Molecular property-binding affinity relationship aspects. *RSC Adv.* **9**(19), 10781–10788 (2019).

37. Mehmood, A. et al. Xanthine oxidase inhibitory study of eight structurally diverse phenolic compounds. *Front. Nutr.* **9**, 966557 (2022).
38. Jiang, L. et al. Hypouricemic effect of gallic acid, a bioactive compound from *Sonneratia apetala* leaves and branches, on hyperuricemic mice. *Food Funct.* **13**(19), 10275–10290 (2022).
39. Sun, Z. R. et al. Ellagic acid exerts beneficial effects on hyperuricemia by inhibiting xanthine oxidase and NLRP3 inflammasome activation. *J. Agric. Food Chem.* **69**(43), 12741–12752 (2021).
40. Wang, Y., Zhang, G., Pan, J. & Gong, D. Novel insights into the inhibitory mechanism of kaempferol on xanthine oxidase. *J. Agric. Food Chem.* **63**(2), 526–534 (2015).
41. Bao, R. et al. Effect of *Eurycoma longifolia* stem extract on uric acid excretion in hyperuricemia mice. *Front. Pharmacol.* **10**, 1464 (2019).
42. Woodward, O. M. ABCG2: The molecular mechanisms of urate secretion and gout. *Am. J. Physiol. Renal Physiol.* **309**(6), F485–F488 (2015).
43. Toyoda, Y. et al. Identification of inhibitory activities of dietary flavonoids against URAT1, a renal urate re-absorber: In vitro screening and fractional approach focused on rooibos leaves. *Nutrients.* **14**(3), 575 (2022).
44 Wang, J. et al. Quercetin protects against cadmium-induced renal uric acid transport system alteration and lipid metabolism disorder in rats. *Evidence-Based Complement. Alternat. Med. eCAM.* **2012**, 548430 (2012).
45. Yang, B. et al. Naringenin ameliorates hyperuricemia by regulating renal uric acid excretion via the PI3K/AKT signaling pathway and renal inflammation through the NF-κB signaling pathway. *J. Agric. Food Chem.* **71**(3), 1434–1446 (2023).
46. Li, F., Liu, Y., Xie, Y., Liu, Z. & Zou, G. Epigallocatechin gallate reduces uric acid levels by regulating xanthine oxidase activity and uric acid excretion in vitro and in vivo. *Ann. Palliat. Med.* **9**(2), 331–338 (2020).
47. Lee, T. H., Chen, J. J., Wu, C. Y., Yang, C. W. & Yang, H. Y. Hyperuricemia and progression of chronic kidney disease: A review from physiology and pathogenesis to the role of urate-lowering therapy. *Diagnostics* **11**(9), 1674 (2021).
48. Wu, Y. L. et al. The extract of *Sonneratia apetala* leaves and branches ameliorates hyperuricemia in mice by regulating renal uric acid transporters and suppressing the activation of the JAK/STAT signaling pathway. *Front. Pharmacol.* **12**, 698219 (2021).
49. Liu, N. et al. Phosphatidylserine decarboxylase downregulation in uric acid-induced hepatic mitochondrial dysfunction and apoptosis. *MedComm.* **4**(4), e336 (2023).
50. Fan, J. et al. Mechanism of gallic acid on LPS-stimulated inflammatory response of macrophages by RNA-Seq technique. *Pharmacol. Clin. Chin/ Mater.* **39**(9), 24–31 (2023).
51 Huang, L. H. et al. Gallic acid inhibits inflammatory response of RAW264.7 macrophages by blocking the activation of TLR4/NF-κB induced by LPS. *Chin. J. Cell. Mol.* **32**(12), 1610–1614 (2016).
52. Aslan, A. et al. Ellagic acid prevents kidney injury and oxidative damage via regulation of Nrf-2/NF-κB signaling in carbon tetrachloride induced rats. *Mol. Biol. Rep.* **47**(10), 7959–7970 (2020).
53. Zhang, B. C., Li, Z., Xu, W., Xiang, C. H. & Ma, Y. F. Luteolin alleviates NLRP3 inflammasome activation and directs macrophage polarization in lipopolysaccharide-stimulated RAW264.7 cells. *Am. J. Transl. Res.* **10**(1), 265–273 (2018).
54. Hossen, I. et al. Epigallocatechin gallate (EGCG) inhibits lipopolysaccharide-induced inflammation in RAW 264.7 macrophage cells via modulating nuclear factor kappa-light-chain enhancer of activated B cells (NF-κB) signaling pathway. *Food Sci. Nutr.* **11**(8), 4634–4650 (2023).
55. Sogo, T. et al. Anti-inflammatory activity and molecular mechanism of delphinidin 3-sambubioside, a Hibiscus anthocyanin. *BioFactors.* **41**(1), 58–65 (2015).
56 Vorobeľová, L. et al. Association of the ESR1 polymorphism with menopause and MLXIPL genetic variant influence serum uric acid levels in Slovak midlife women. *Menopause.* **26**(10), 1185–1192 (2019).
57. Liu, R. et al. Prevalence of hyperuricemia and gout in Mainland China from 2000 to 2014: A systematic review and meta-analysis. *BioMed Res. Int.* **2015**, 762820 (2015).
58. Takiue, Y., Hosoyamada, M., Kimura, M. & Saito, H. The effect of female hormones upon urate transport systems in the mouse kidney. *Nucleosides Nucleotides Nucl. Acids.* **30**(2), 113–119 (2011).
59. Budhiraja, R. et al. Estrogen modulates xanthine dehydrogenase/xanthine oxidase activity by a receptor-independent mechanism. *Antioxidants Redox Signal.* **5**(6), 705–711 (2003).
60. Khaled, S. E. et al. A biochemometric approach for the assessment of *Phyllanthus emblica* female fertility effects as determined via UPLC-ESI-qTOF-MS and GC-MS. *Food Funct.* **10**(8), 4620–4635 (2019).
61. Schuit, S. C. et al. Estrogen receptor alpha gene polymorphisms are associated with estradiol levels in postmenopausal women. *Eur. J. Endocrinol.* **153**(2), 327–334 (2005).
62. Efstathiadou, Z. A. et al. Associations of estrogen receptor alpha and Beta gene polymorphisms with lipid levels and insulin resistance in men. *Metab. Clin. Exp.* **64**(5), 611–617 (2015).
63. Ahmed, F. et al. Role of Estrogen and its receptors in adipose tissue glucose metabolism in pre- and postmenopausal women. *J. Clin. Endocrinol. Metab.* **107**(5), e1879–e1889 (2022).

Acknowledgements

This work was supported by National Natural Science Foundation of China (81603669), Natural Science Foundation of Guangdong Province (2021A1515010978 and 2021A1515012474), Basic research project of Shenzhen Science and Innovation Commission (JCYJ20210324121610029) and Guangdong Provincial Key Areas Research and Development Program project Lingnan TCM Modernization (2020B1111120003).

Author contributions

L. and Z. designed the research project; W. and X. performed the experiments; J. analyzed the data; L. and Z. wrote the manuscript.

Declarations

Competing interests

The authors declare no competing interests.

Additional information

Supplementary Information The online version contains supplementary material available at https://doi.org/10.1038/s41598-024-79350-x.

Correspondence and requests for materials should be addressed to Q.J. or Y.Z.